
Investigating potential icequakes at Llaima volcano, Chile

Oliver D. Lamb^{1,*}, Jonathan M. Lees¹, Luis Franco Marin², Jonathan Lazo^{2,3},
Andrés Rivera⁴, Michael J. Shore¹, and Stephen J. Lee⁵

¹*Department of Geological Sciences, University of North Carolina at Chapel Hill, Chapel Hill, NC, USA*

²*OVDAS-Sernageomin, Chilean Geological Survey, Chile*

³*Department of Physical Sciences, University of La Frontera, Temuco, Chile*

⁴*Departamento de Geografía, Universidad de Chile, Chile*

⁵*U.S. Army Research Laboratory/Army Research Office, Research Triangle Park, NC, USA*

Correspondence*:

O. D. Lamb

olamb@email.unc.edu

2 ABSTRACT

3 Glacially- and magmatically-derived seismic events have been noted to heavily overlap in
4 characteristics, thus there exists the potential for false-alarms or missed warnings at ice-covered
5 volcanoes. Here we present the first study to specifically investigate icequakes at an ice-covered
6 volcano in Southern Chile. Two months of broadband seismic data collected at Llaima volcano
7 in 2015 were analyzed in order to quantify, characterize, and locate potential glacially-derived
8 seismic events at one of the most active ice-covered volcanoes in the region. We find over
9 1,000 repeating seismic events across 11 families, the largest of which contains 397 events.
10 Approximate locations and characteristics of the largest families lead us to conclude that these
11 events were derived from persistent stick-slip motion along the ice-rock interface at the base of a
12 glacier near the volcano summit. These results have implications for future seismic monitoring at
13 Llaima volcano and other ice-covered active volcanoes in the region.

14 **Keywords:** Volcano-seismology, Cryoseismology, Llaima volcano, Monitoring, Repetitive

15 RESUMEN

16 Se ha observado que los fenómenos sísmicos derivados de los glaciares y magmáticos se
17 superponen en gran medida en las características, por lo que existe la posibilidad de que se
18 produzcan falsas alarmas o de que se pasen por alto las alertas en los volcanes cubiertos de
19 hielo. Aquí presentamos el primer estudio que apunta específicamente a los terremotos en un
20 volcán cubierto de hielo en el sur de Chile. Se analizaron dos meses de datos sísmicos de banda
21 ancha recolectados en el volcán Llaima en 2015 para cuantificar, caracterizar y localizar eventos
22 sísmicos derivados de glaciares en uno de los volcanes cubiertos de hielo más activos de la
23 región. Encontramos más de 1,000 eventos sísmicos repetidos en 11 familias, el más grande de
24 los cuales contiene 397 eventos. Las ubicaciones y características aproximadas de las familias
25 más grandes nos llevan a la conclusión de que estos eventos se derivaron de un movimiento

26 persistente de stick-slip a lo largo de la interfase de la roca de hielo en la base de un glaciar cerca
27 de la cima del volcán. Estos resultados tienen implicaciones para el futuro monitoreo sísmico en
28 el volcán Llaima y otros volcanes activos cubiertos de hielo en la región.

1 INTRODUCTION

29 For volcano monitoring organizations a fundamental goal is to assess whether changes in seismicity
30 indicates impending intensification of volcanic eruptive activity. Earthquakes generated by magma
31 movement beneath volcanoes are recorded across a wide range of waveform shapes and frequencies
32 (Chouet and Matoza, 2013). Low-frequency earthquakes linked to volcanic activity are traditionally thought
33 to be generated by the resonance of fluid-filled cracks (e.g. Chouet, 1996), but may also be linked to
34 slow-rupture failure of magma or volcanic materials (e.g. Neuberg et al., 2006; Iverson et al., 2006; Bean
35 et al., 2013). However, seismicity generated by glaciers can often resemble signals associated with fluid
36 or magma transport within volcanoes (Weaver and Malone, 1976; West et al., 2010). There are multiple
37 documented processes for generating seismicity around glaciers, including crevassing, ice-fall events,
38 stick-slip motion at the base, hydrofracturing within the ice, and subglacial water flow (Podolskiy and
39 Walter, 2016; Aster and Winberry, 2017). In addition, the interaction of meltwater from ice or snow with
40 magmatic hydrothermal fluids can generate shallow low-frequency seismicity (e.g. Matoza et al., 2015;
41 Park et al., 2019). Most or all of these mechanisms have been documented or surmised to occur in case
42 studies at multiple glacial volcanoes (Weaver and Malone, 1976; Métaxian et al., 2003; Caplan-Auerbach
43 and Huggel, 2007; Jónsdóttir et al., 2009; Thelen et al., 2013; Allstadt and Malone, 2014).

44 Glacial signals are usually weak and therefore only recorded at stations close to the source (Weaver
45 and Malone, 1976), but there are documented examples of glaciers producing earthquakes as large as
46 magnitude 5 (Ekstrom et al., 2003) and/or being recorded at considerable distance from the source
47 (e.g. Caplan-Auerbach and Huggel, 2007). Most cases of documented glacial signals describe a strong
48 attenuation of higher frequencies between the source and receiver (Weaver and Malone, 1979; Métaxian
49 et al., 2003; Thelen et al., 2013; Allstadt and Malone, 2014) and/or longer duration slip proportional to
50 magnitude (Ekstrom et al., 2003). In addition, signals derived from glacial sources on volcanoes have
51 often had a strongly repetitive nature which may persist on timescales of months to years (Jónsdóttir et al.,
52 2009; Allstadt and Malone, 2014). Repetitive glacially-derived seismic events are also commonly seen
53 beneath glaciers in non-volcanic contexts (e.g. Danesi et al., 2007; Helmstetter et al., 2015; Roeoesli
54 et al., 2016). This presents another overlap in characteristics with volcanic earthquakes since repetitive low
55 frequency events associated with magma movement and failure have been documented prior to or during
56 multiple eruptions (e.g. Iverson et al., 2006; Kendrick et al., 2014; Lamb et al., 2015). As an example for
57 the potential issues of this confusion, careful analysis of seismic data revealed 150,000 low-magnitude
58 ($M < 1$), low-frequency repeating events at Mt. Rainier which were interpreted as caused by basal stick-slip
59 motion beneath the glaciers on the volcano (Allstadt and Malone, 2014). The low-frequency and repetitive
60 nature of these seismic events closely resembled seismicity often seen prior to or during eruptive activity at
61 volcanoes around the world (Thelen et al., 2013). Therefore, the ability to distinguish between glacial and
62 volcanic sources is vital for providing correct and rapid interpretations of seismicity at active glacier-clad
63 volcanoes.

64 Here we present a detailed analysis of broadband seismic data collected at Llaima volcano during a
65 temporary deployment in early 2015, with a primary focus on assessing the prevalence of icequakes. Llaima
66 volcano is one of the most active volcanoes in Southern Chile and host to multiple glaciers on the upper
67 flanks. This is the first known study to focus primarily on glacial seismic events on active volcanoes in

68 Southern Chile. We detail several sequences of repetitive low-frequency seismic events at the volcano over
 69 the course of two months, and propose that these are of glacial rather than volcanic origin.

2 LLAIMA VOLCANO

70 Southern Chile is home to a chain of active ice-covered volcanoes, the most active of which is Llaima
 71 volcano (Fig. 1). Llaima is a complex stratovolcano and one of the largest in the region (377 km^3 , 3179 m
 72 a.s.l.; Völker et al., 2011) and largely composed of basaltic to andesitic composition lavas (de Maisonneuve
 73 et al., 2012). Up to 54 documented eruptions have occurred at the volcano since the 17th century (Naranjo
 74 and Moreno, 2005; Franco et al., 2019). The most recent episode, from 2007 to 2009, was the strongest
 75 since the 1950's with ash columns reaching 7 km above sea level and lahars generated by melting glacial
 76 ice (Franco et al., 2019).

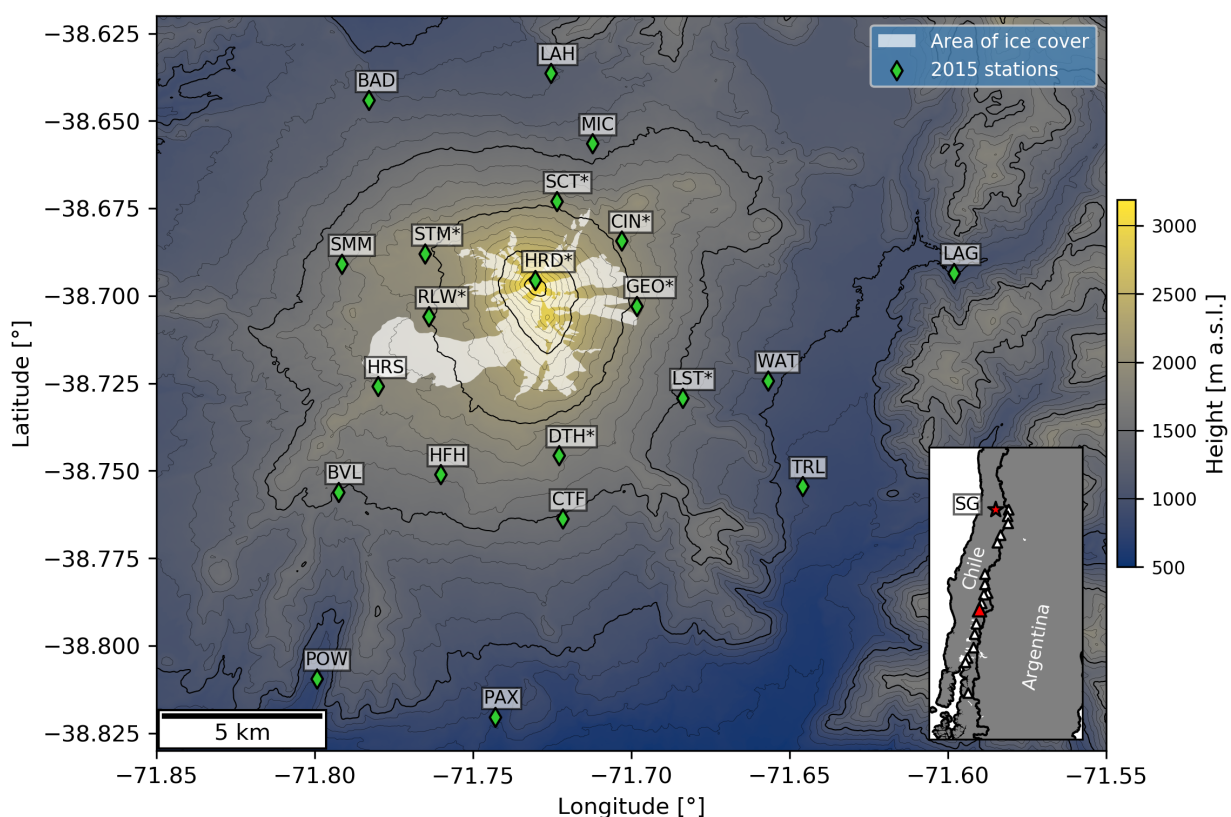


Figure 1. Map of Llaima volcano with the locations of the 2015 seismic stations used in this study marked with green diamonds (5 of the 26 stations are not visible). Names marked with asterisks (*) were those used in the STA/LTA method described in Section 3. Also marked are the mapped summit glacial areas marked as ‘clear’ or ‘debris-covered’ ice (white area). Thick and thin contours mark 500 and 100 m altitude intervals, respectively. Inset: Map of Southern Chile with the location of Llaima volcano (red triangle) and Santiago (red star, SG) marked. Also plotted are the locations of other ice-covered volcanoes within the Southern Volcanic Zone of Chile that have displayed eruptive activity in last 200 years (white triangles; Venzke, 2013).

77 The glacial area presented in this study (white area in Fig. 1) was calculated by using high-resolution
 78 (0.5 m pixel size) Digital Globe panchromatic satellite image taken on March 6 2016. This image was
 79 georeferenced to geographical coordinate system using WGS1984 datum yielding an estimated horizontal
 80 accuracy of 1-2 pixels. The image was manually analyzed following the methods presented by Paul et al.

81 (2013) allowing identifying areas of ice that were classified as either ‘clear ice’, ‘debris-covered ice’, or
82 ‘unclear’. These categories were defined by characterizing the surface patterns where clear ice polygons
83 are bright snow or ice surfaces with or without crevasses and little debris cover material. The albedo is
84 high for snow and lower when bare ice is present. Sometimes the ground area is slightly brown due to
85 minor surface material. The ‘debris-covered ice’ class was assigned when surface debris form patterns
86 indicating that underlying ice was present. Such patterns could be formed by the presence of crevasses
87 ice-cliff backwasting, undulations, or morrenic-like alignments. Finally, unclear areas were selected when
88 surface patterns were similar to inactive rock glaciers but without crevasses or other features indicating ice
89 dynamic were observed. The spatial resolution of the utilized image (0.5 m) was very good for detecting
90 very small features like erratic blocks, small crevasses and other glacier origin forms. This resolution
91 allowed estimating the total glacial area on Llaima volcano with higher detail than previous work. This
92 explains why our estimate is significantly larger than 5.5 km² estimated by Reinthaler et al. (2019), that
93 used Landsat 8 OLI images (15 m pixel size for band 8) in which debris-covered ice would not be clear.
94 Nevertheless, it is clear from satellite images that the glacial area at Llaima volcano has been significantly
95 reduced in recent decades due to eruptive activity and global climate change (Reinthaler et al., 2019).

96 To provide a degree of security for nearby population centers, OVDAS (Observatorio Vulcanológico
97 de los Andes Sur¹) has deployed a network of stations around the volcano to continuously monitor its
98 activity. OVDAS use the criteria described in Lahr et al. (1994), Chouet (1996), and Chouet and Matoza
99 (2013) to identify and classify the earthquakes recorded by the seismic network around the volcano. Arrival
100 times and waveform amplitudes are used to differentiate between volcanic and tectonic events. Using a
101 reference station within the network, the volcanic earthquakes are classified as volcano-tectonic, long-period
102 (including hybrid), or tremor events. Each type of earthquake has been associated with multiple distinct
103 source mechanisms and relative temporal trends of each type has important implications for assessing the
104 activity state of a volcano (see Chouet and Matoza, 2013, and references therein). OVDAS also manually
105 distinguishes other non-volcanic or non-tectonic events such as cryogenic earthquakes, but have no mandate
106 to track these events therefore little is known about their prevalence in the seismic record (Mora-Stock et al.,
107 2014). Recent studies have attempted to construct automatic event classifiers for Llaima volcano using
108 machine learning algorithms for pattern recognition with varying degrees of success (Curilem et al., 2014,
109 2018; Soto et al., 2018). However, these studies either grouped the few identified cryogenic earthquakes
110 with other earthquake types (Curilem et al., 2014), or excluded them from their training databases (Curilem
111 et al., 2018; Soto et al., 2018). Therefore, the databases may have included a mixture of glacially- and
112 magmatically-derived earthquakes that could have had an impact on their results. Before further automatic
113 event classification algorithms are deployed for Llaima volcano, it is clear there exists a need to constrain
114 the preponderance of cryogenic earthquakes in the seismic record.

115 **2.1 2015 deployment**

116 From January to March 2015, twenty-six broadband seismic stations were deployed across an
117 approximately 30 x 20 km area centered on Llaima volcano as part of a UNC Chapel Hill, Boise State
118 University and Southern Andes Volcano Observatory (OVDAS) collaboration (Fig. 1). Application of
119 receiver function analysis to this seismic data revealed a low-velocity zone at 8-13 km depth beneath the
120 volcano that could be interpreted as a magmatic body (Bishop et al., 2018). The network used a variety of
121 broadband seismometers that used various digitizers recording the data at 100 samples per second, see
122 Table S1 for specific details of what each station used.

¹ part of Servicio Nacional de Geología y Minería (SERNAGEOMIN)

3 GENERATING A CATALOG OF CANDIDATE ICEQUAKES

123 To detect candidate seismic events at Llaima volcano, we applied a multistation detection algorithm on
124 seismic data collected from 1 February to 31 March 2015. Trigger times were extracted from multiple
125 stations using a short-term average/long-term average algorithm (STA/LTA), on condition that an event
126 was detected coincidentally in time at ≥ 2 stations. We used lengths of 1 and 9 s for the short and long
127 time windows, respectively, and a ratio of 5 was used to define a detected event; these parameters were
128 decided by manual inspection of events detected over 24 hours of seismic data recorded at station GEO.
129 Considering the low magnitude and strong attenuation noted for icequakes at other volcanoes (e.g. Allstadt
130 and Malone, 2014), we used only the eight closest stations to the summit for this step (marked by asterisks
131 in Fig. 1 and Table S1). Seismic data were preprocessed with a bandpass filter of 0.5-10 Hz to improve the
132 signal-to-noise ratio (SNR).

133 From the catalog of candidate triggers compiled by the multi-station detection algorithm, our next step
134 was to find seismic events that were repetitive over the period of study. In order to reduce the computing
135 load, we followed a similar methodology to that detailed by Allstadt and Malone (2014) who used an
136 algorithm modified from Carmichael (2013). The method uses unsupervised clustering of seismic events so
137 the user does not need to define templates in order to detect repeating events. First, we cross-correlate every
138 event with all other events within each day and group them into families, using a minimum cross-correlation
139 coefficient of 0.7 to define two events as a match; we use the `scipy.cluster.hierarchy` Python package to carry
140 out this step (see <https://docs.scipy.org/doc/scipy/reference/> for more details, last accessed 7 February 2020).
141 For each event, we used the first 5 s of the waveform, sufficient to include the largest wave amplitudes
142 while minimizing the contribution of background noise. Seismograms from station GEO were used to build
143 the catalog, as this station had the highest number of detected events. Families of repeating waveforms were
144 defined using a hierarchical clustering method similar to that used by Buurman and West (2013) and Lamb
145 et al. (2015). Next, a median waveform stack is computed for each family of 2 events or more detected each
146 day. Each stack is then compared to all other stacks across the whole time period to find larger, multi-day
147 families. Finally, in order to ensure the repeating event catalog is as complete as possible we scan the entire
148 time period with a stacked waveform from each multi-day family in order to find any events potentially
149 missed in the previous steps. For this step, we used the super-efficient cross-correlation algorithm (SEC-C),
150 a frequency domain method that optimizes computations using an overlap-add approach, vectorization, and
151 fast normalization (Senobari et al., 2019).

4 RESULTS

152 4.1 Catalog of low-level seismic activity

153 Between 1 February and 31 March 2015, we detected 4,894 seismic events at Llaima volcano (dashed
154 grey bars in Fig. 2a). This value is significantly larger than the 572 seismic events that were manually
155 cataloged by OVDAS during the same period (red dash-dot line in Fig. 2a). The OVDAS catalog includes
156 490 seismic events dominated by low-frequency volcanic events (a.k.a. long-period) and 82 surface activity
157 such as avalanches (Fig. S1). Using the catalog of automatically detected events, we identified 1,134
158 repeating seismic events that were divided across 11 different families (Fig. 2a, c). Of the 490 events
159 cataloged as long-period events, only 2 matched with detected repeating seismic events (Fig. S2). The
160 largest of these families included 396 events, with repose intervals of 1 to 15 hours. The rate of daily
161 seismic event rates, including repeating seismic events, are relatively continuous throughout the period of
162 study with no obvious indications of cyclic activity or significant changes in rates. Weather data collected at

163 a station situated in the town of Melipeuco (approximately 17 km SSE from the volcano summit) indicates
 164 no significant rainfall or temperature fluctuations in the area during the period of study (Fig. 2b).

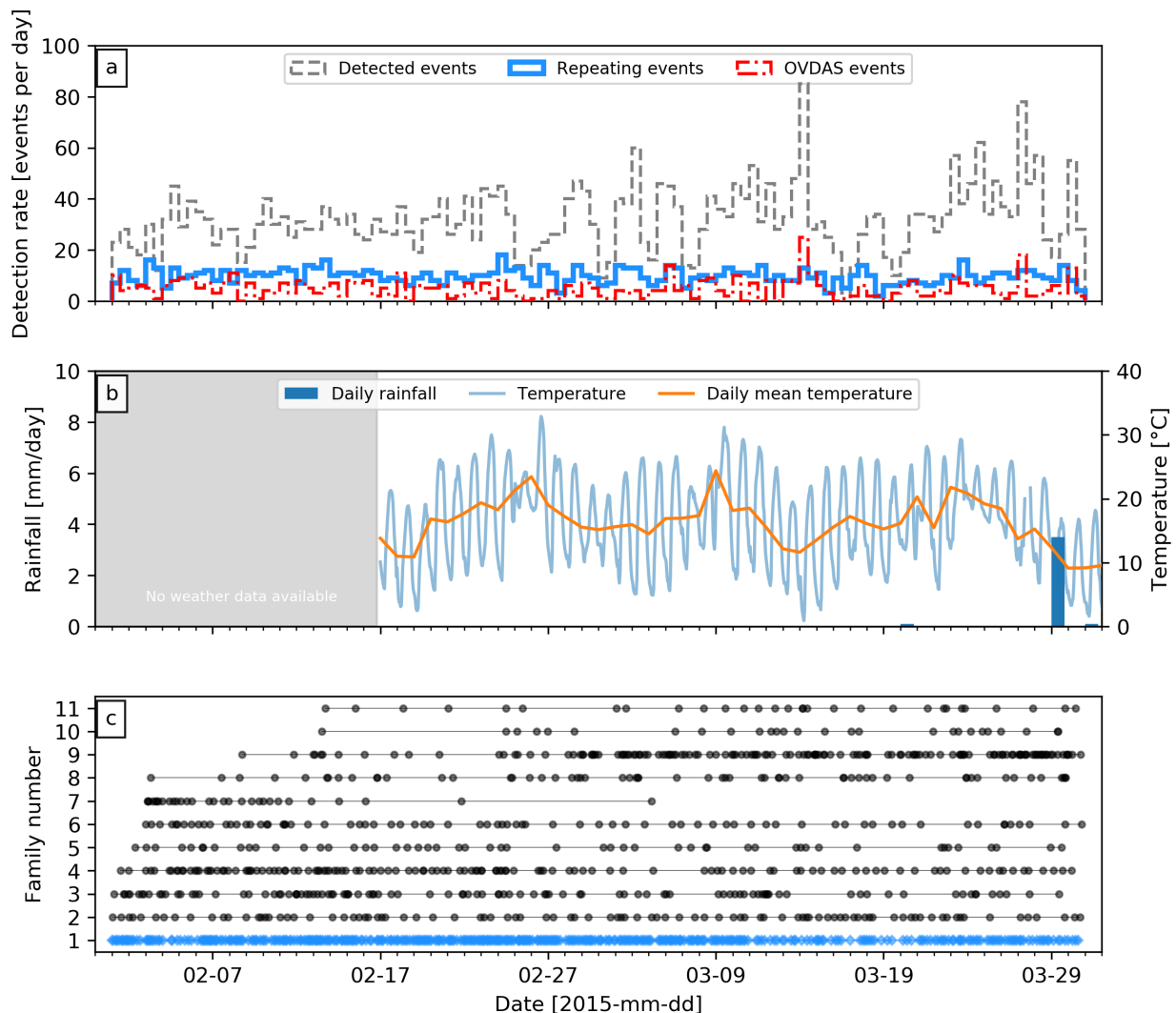


Figure 2. (a) Rates for events automatically detected (grey dashed bars), events classified as repeaters (red solid bars), and seismic events manually classified by OVDAS (red dashed bars) from 1 February to 31 March 2015 in 12-hour bins. (b) Daily events in rainfall (blue bars) and variations in temperature on an hourly (light blue) and daily rate (orange line). (c) Catalog of family occurrence in our dataset. Each plotted point represents the time of an event, and lines join events from the same family. The largest family (Family 1) is plotted using blue diamonds for the individual events.

165 4.2 Characteristics of repeating seismic events

166 The earthquakes allocated to the largest family of repeating events (henceforth called Family 1) are
 167 generally small, with magnitudes of less than 1, and appear to be of an emergent low-frequency nature (Fig.
 168 3a). However, the low-frequency and emergent nature of these events were likely the result of path effects
 169 as the waves were strongly altered and attenuated as they traveled away from the volcano (Fig. 4a). To
 170 compare the relative magnitudes of events within the family, we calculate the pseudo-energy for each event
 171 waveform, which is the integral of the Hilbert envelope of the waveform (Rowe et al., 2002; Thelen et al.,

172 2013). For Family 1, there is a weak linear relationship between the repose interval between events and the
 173 pseudo-energy of the subsequent seismic event (Fig. 3b); this characteristic is not shared across most of the
 174 other families detected (Fig. S3-S5). When events in each family are binned by time-of-day occurrence,
 175 there are few, if any, significant correlations with time of day or temperature (Fig. S6). However, it's likely
 176 that the families here do not contain enough events for any significant relationships to become visible, due
 177 to the relatively short length of the time analyzed.

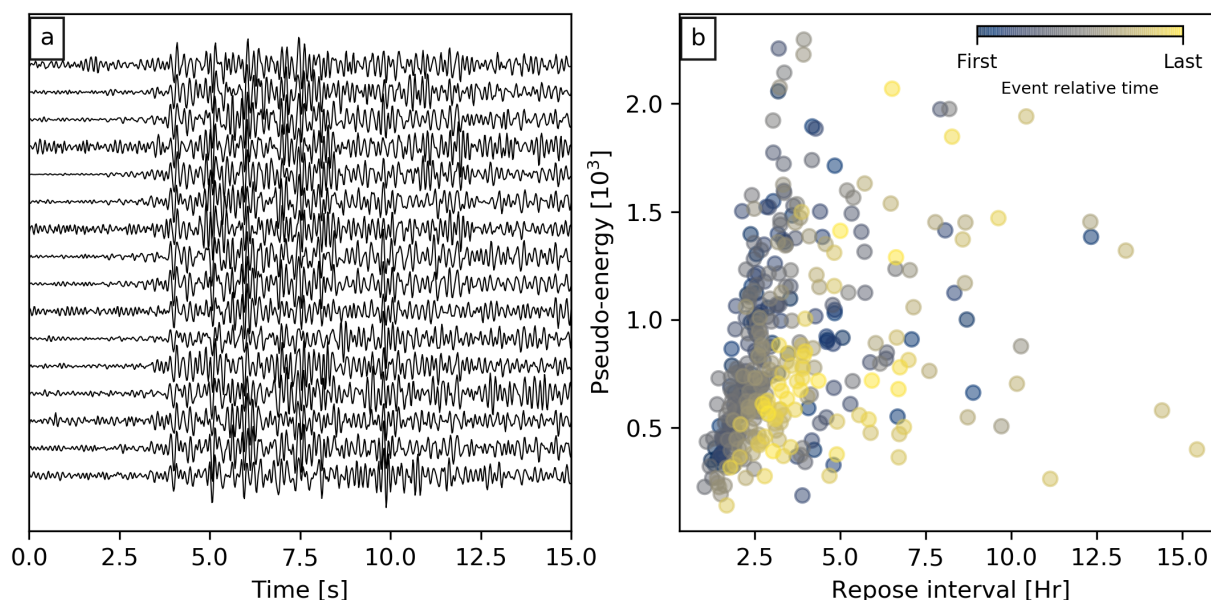


Figure 3. (a) Waveforms of the first 15 events in Family 1, as recorded at station GEO. Each waveform is normalized to their maximum amplitude, and plotted in order of their occurrence from the top. (b) Repose intervals versus pseudo-energy for each event in Family 1, colored by their relative age within the family duration, using waveforms recorded at station GEO.

178 4.3 Location of largest families

179 Calculating the source locations for each of the families is crucial for understanding the source
 180 mechanism(s) involved. However, locating individual events within each family detected at Llaima
 181 volcano without unacceptable error margins is impossible due to the emergent and low SNR nature of
 182 each waveform, as well as the rapid attenuation of the signal as it moves away from volcano (Fig. 4a).
 183 Nonetheless, following Allstadt and Malone (2014), we can take advantage of the repeating nature of
 184 these families and calculate median stacks for each family at each station. If there are enough events in the
 185 family, clearer signals with relatively high SNR can be acquired on at least 3 stations in the network (Fig.
 186 4b). The improvement in the SNR is such that relative P-wave arrival times across the station can be used
 187 for a grid-search location algorithm. In addition, we can also determine the direction of first motions at 9
 188 of the closest stations to the volcano summit for Family 1 (Fig. 5). The first motions for Family 1 in the
 189 vertical component show mixed polarities across these stations. However, the stacking method only applied
 190 for three families, as the SNR did not improve enough for clear P-wave arrivals in the remaining families.

191 Once the P-wave arrival times were picked, we used a brute-force 3D grid-search algorithm to estimate
 192 source locations. This method uses the relative arrival times between the first recorded arrival and all
 193 subsequent arrival times to find the most appropriate source location using a fixed P-wave velocity value.

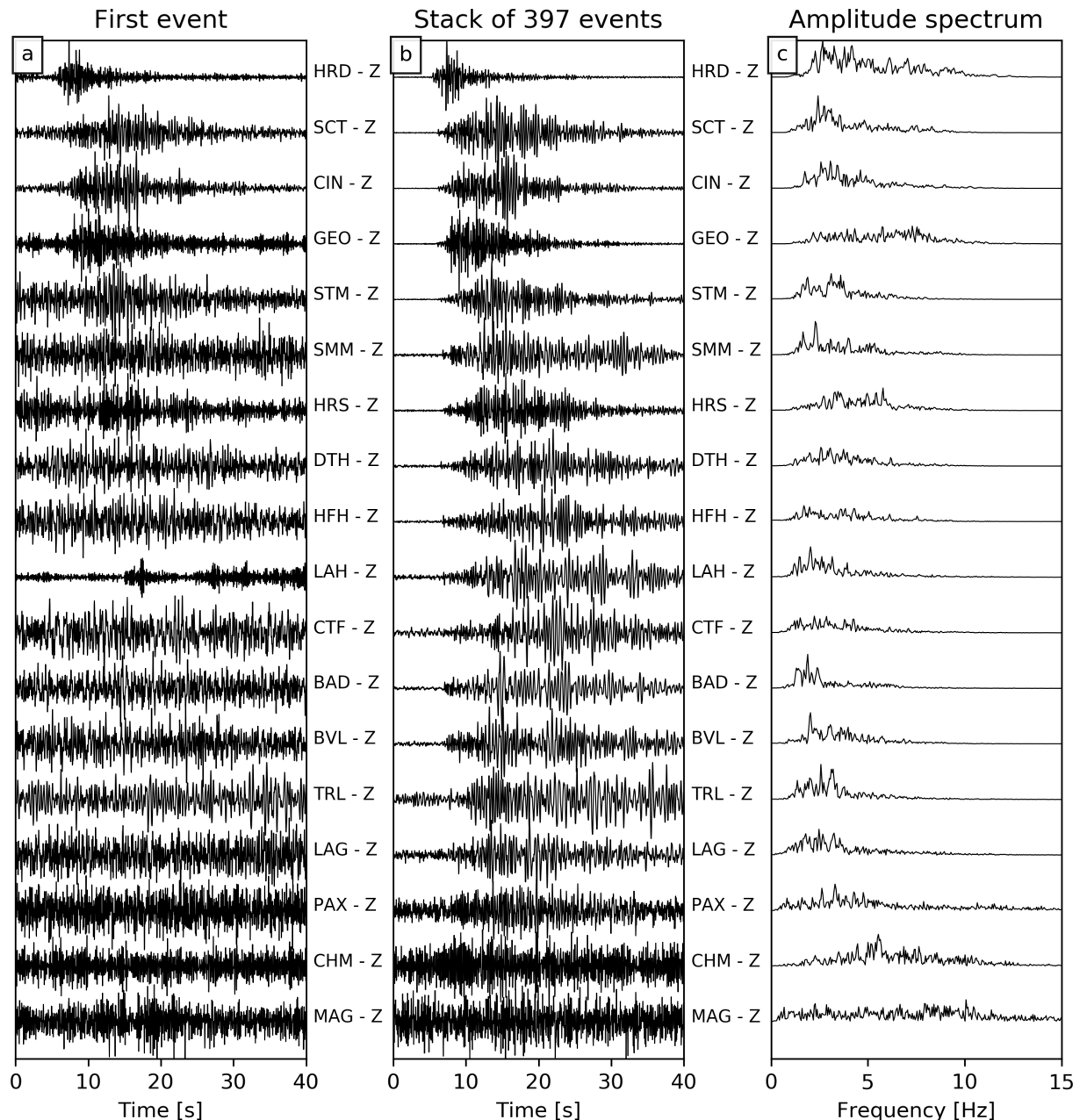


Figure 4. (a) The waveform of the first detected event in Family 1 as recorded at stations within the 2015 deployment, ordered by distance from the summit. (b) Stacked waveforms generated from the 397 events detected in Family 1 at each station. (c) Normalized frequency-amplitude spectra of the stack waveforms presented in panel (b).

194 In other words, artificial relative arrival times are calculated for each point in the grid, and compared to the
 195 real relative arrival times. The location is that which most closely matches the real relative arrival times.
 196 We defined the grid of source nodes using a 29 m horizontal and 37 m vertical resolution. A previous study
 197 used a seismic velocity of 2.5 km s^{-1} for the surface layer to calculate seismic power for continuous tremor
 198 recorded during the 2007-2009 eruptive period (Franco et al., 2019). A compilation of seismic velocity
 199 profiles for andesitic-basaltic volcanoes suggest that P-wave velocities range from approximately 0.5 km s^{-1}
 200 at the surface up to 6 km s^{-1} at 4 km depth (Lesage et al., 2018). Crustal models developed by OVDAS for

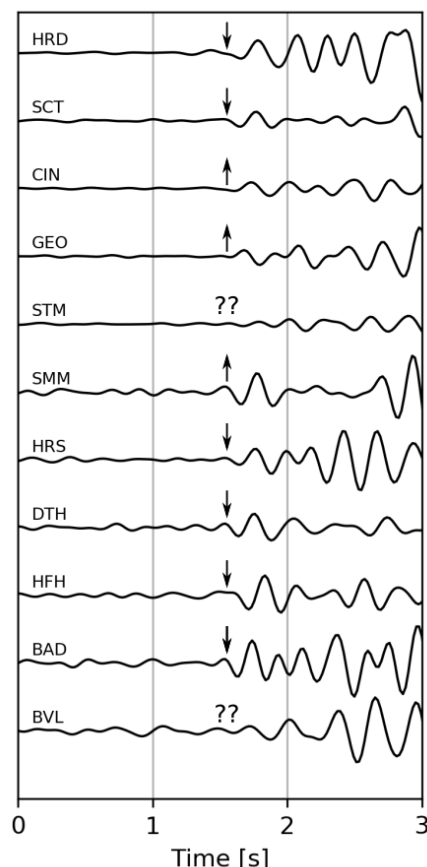


Figure 5. First arrivals of stacked waveforms of Family 1 as recorded by 11 stations in the 2015 network, bandpass filtered at 2-5 Hz. Where the first motion is uncertain, they have been marked with question marks. The waveforms here have been manually realigned to approximately the same arrival time for the purpose of this plot.

201 several volcanoes, including Llaima volcano, use a seismic velocity of 4 km s^{-1} for the upper layer of the
 202 volcanic edifice. Therefore, for our grid search we used a fixed value of 4 km s^{-1} .

203 The locations of the three largest families from which we could get enough clear P-wave arrival times
 204 are plotted in Figure 6. The locations of each family is tightly clustered around the summit vent, near or
 205 beneath the top of the glaciers. The depths of each family is very shallow, on the order of 10's of meters.
 206 However, it is important to note that the uncertainties in these locations are very high due to a number of
 207 factors. The use here of a 1-D velocity model is likely not appropriate for what is a very heterogeneous
 208 edifice. Furthermore, any slight misalignment of waveforms during stacking will introduce errors to the
 209 picked P-wave arrival times at each station. Errors may also be introduced during the manual picking of
 210 the P-wave arrival times. Lastly, the spacial resolution used during the brute-force grid-search algorithm
 211 enforces a minimum in the expected errors of the locations. Therefore, the locations presented here are
 212 a rough approximation of the actual source positions, with approximate errors on the order of $\pm 500 \text{ m}$
 213 laterally and vertically. Nevertheless, it is clear from the waveform arrival times across the network (e.g.
 214 Family 1; Fig. 4a,b) that the source locations were nearest to station HRD and therefore close to the volcano
 215 summit. For other families where not enough clear arrivals were acquired to calculate locations, it is clear
 216 that some are located closer to station GEO instead of HRD (e.g. Family 3, 6 and 7; Fig. S8, S11, and S12,

217 respectively). This indicates that the source locations for these families would be close to or beneath the
 218 termini of mapped glacial areas in the east and north-east flanks of the volcano.

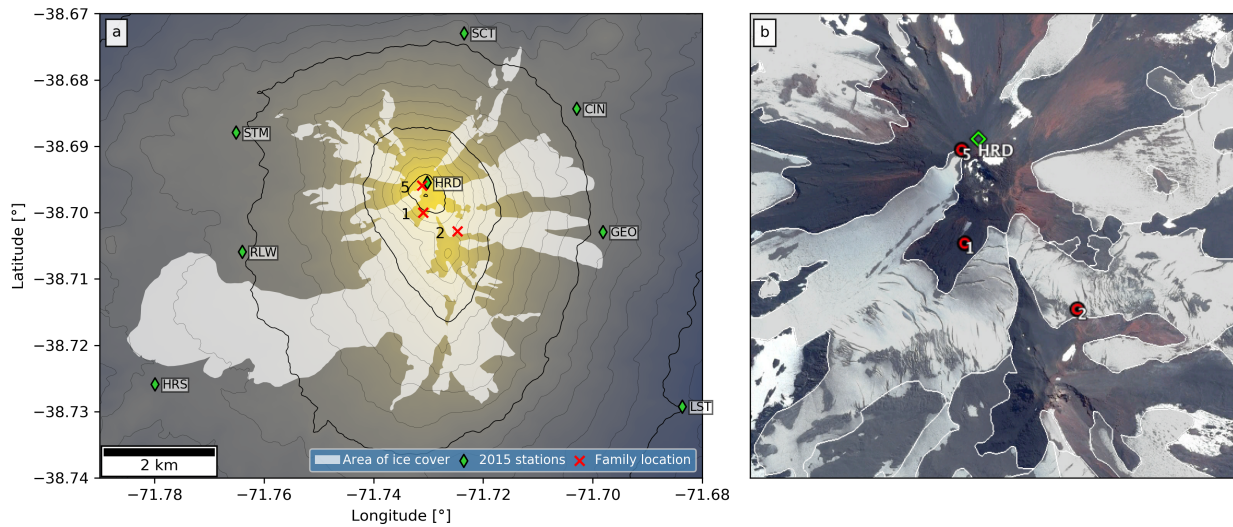


Figure 6. (a) Map of Llaima volcano summit area with the locations of the closest 2015 seismic stations used in this study marked with green diamonds. Also marked are the summit glacial areas (white area), as well as locations of three families (red crosses). Thick and thin contours mark 500 and 100 m altitude intervals, respectively. Colormap used is identical to that used in Fig. 1. (b) Satellite image of the summit area of Llaima volcano, with station HRD marked (green diamond) and the locations of the largest three families (red circles). Also marked are the mapped glacial areas (white areas). Image source: Google-CNRS-Airbus-Digital Globe, captured on March 6 2016.

219 4.4 Source locations over time

220 While it may not be possible to calculate exact source locations, coda wave interferometry (CWI) can
 221 use the repeating waveforms within each family to provide an estimate of source separation during the
 222 lifetime of the family (i.e. source location drift). Any migration in a repeating seismic source (or change in
 223 the seismic velocity properties of the medium) results in a change in distance (or velocity) to scatterers
 224 in the surrounding medium, which in turn affects the arrival times of phases in the waveform coda. Here
 225 we are assuming there was no change in the locations of scatterers in the medium. Allstadt and Malone
 226 (2014) used CWI to demonstrate drifts of up to 7 meters per day for the locations of repeating icequakes at
 227 Mt. Rainier volcano. Here, we use a similar approach on Family 1 to elucidate whether any drift may be
 228 occurring at the source location.

229 The correlation coefficient between waveforms, R , is related to the variance of the travel-time perturbation,
 230 σ_τ according to the following relationship (Snieder et al., 2002):

$$R = 1 - \frac{1}{2}\bar{\omega}^2\sigma_\tau^2 \quad (1)$$

231 where the mean-squared frequency, $\bar{\omega}^2$, can be calculated from the seismogram data, $u(t)$:

$$\bar{\omega}^2 = \frac{\int_{t-T}^{t+T} \dot{u}^2(t') dt'}{\int_{t-T}^{t+T} u^2(t') dt'} \quad (2)$$

232 where the integral is performed over a window of length $2T$ centered at time t and \dot{u} is the time derivative
 233 of the waveform, u . We also apply a correcting factor to R to account for bias due to noise in the waveforms
 234 (Douma and Snieder, 2006). The relationship between the variance of the travel-time perturbation and
 235 inferred source migration depends on the source mechanism, such as explosive, point, or fault-plane
 236 (Snieder and Vrijlandt, 2005). Evidence from the mixed first-motion polarities (Fig. 5) suggest that it is
 237 reasonable to assume, for the purposes of this calculation, that the source is dominated by shear motion
 238 along a fault-plane. Therefore, if displacement occurs along a fault-plane, the source dislocation between
 239 waveforms, δ , is given by:

$$\delta = \left[7 \left(\frac{2}{v_p^6} + \frac{3}{v_s^6} \right) / \left(\frac{6}{v_p^8} + \frac{7}{v_s^8} \right) \right]^{\frac{1}{2}} \sigma_\tau \quad (3)$$

240 where v_p and v_s are the P- and S-wave velocities in the medium. Note that using different seismic
 241 velocities or different source mechanisms will change the displacement magnitude, but not the pattern of
 242 movement over time. Lesage et al. (2018) compile measurements of v_p/v_s ratios for andesitic basaltic
 243 volcanoes that approximately range from 1.5 to 2.5. Here we calculate displacements using P-wave
 244 velocities ranging from 1 - 4 kms^{-1} , with a v_p/v_s ratio of 2. As the individual waveforms within Family 1
 245 have relatively low SNR, we instead apply CWI to stacked subsets of the family in order to improve the
 246 SNR. Family 1, featuring 397 events, was divided up into 13 subsets of 30 or 31 events, and median stacks
 247 were calculated from each stack. R was calculated using 8 second windows starting 5 s after the start of the
 248 stacked waveform, bandpass filtered at 1-10 Hz, for each stack relative to the first stack, and converted to δ .

249 For Family 1, the calculated displacements from waveforms recorded at two different stations (HRD,
 250 GEO) are <1 m/day (Fig. 7). The largest displacements appear to occur during the first part of the recorded
 251 family lifespan, before it stabilizes during the rest of the study period. Total source displacements at the
 252 highest v_p values used (4 kms^{-1}) are still significantly lower than what has been observed at other volcanoes
 253 (e.g. Mt. Rainier; Allstadt and Malone, 2014). While the displacements between each station may differ, the
 254 overall shape of the calculations are relatively similar which lends credibility to the calculations presented
 255 here.

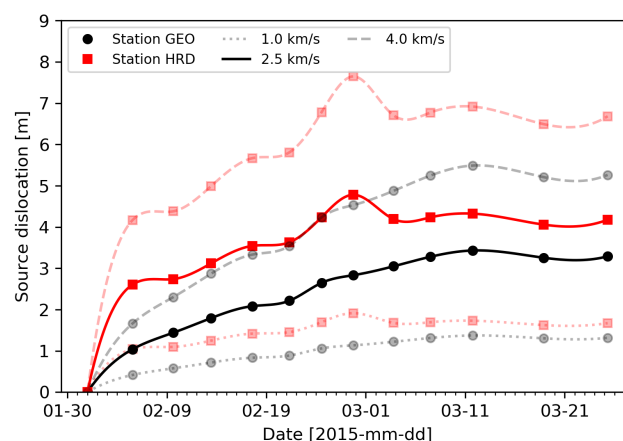


Figure 7. Calculated source displacements for Family 1 at stations GEO (black) and HRD (red). Solid lines are estimates using v_p of 2.5 km^{-1} with dotted lines indicating the lower (1 km^{-1}) and upper (4 km^{-1}) bounds of possible seismic velocities.

5 DISCUSSION

256 Here we have presented results of analysis of broadband seismic data collected at Llaima volcano in 2015,
257 with the aim of understanding the preponderance for icequake activity at the volcano. While previous
258 studies have noted the presence of icequakes in the seismic record at the volcano (e.g. Curilem et al., 2014;
259 Mora-Stock et al., 2014), they are apparently relatively rare compared to other ice-covered volcanoes
260 (Métaxian et al., 2003; Jónsdóttir et al., 2009; Allstadt and Malone, 2014). Indeed, during our study period,
261 OVDAS officially cataloged no icequakes as it is not within their mandate to do so (Fig. S1). While we
262 study a relatively small time period, from our observations described above we would argue that glacially
263 derived seismic events may be far more prevalent in the seismic record than previously thought.

264 We conclude that the low-frequency and repetitive seismic activity detailed here is caused by glacial
265 movements on the flanks of Llaima volcano, for the following reasons: 1) No magmatic activity was
266 observed at the volcano during the study period, and not since 2010. Therefore, no magmatically related
267 source mechanisms can be inferred. 2) Despite only looking at two months of seismic data, it is clear that
268 the repetitive families are persistent and long-lasting, which might be expected for glacially derived seismic
269 events (e.g. Jónsdóttir et al., 2009; Allstadt and Malone, 2014). 3) The waveforms seen here share many
270 characteristics as previously described icequakes at other volcanoes, i.e. low-amplitude, rapid attenuation.
271 4) The locations for three of the families, including the largest, place them close to or beneath glaciers near
272 the summit of the volcano.

273 There exist other potential sources for low-frequency seismicity at volcanoes that are not directly related
274 to magmatic activity or glacial motion. The movement of hydrothermal fluids through the system could
275 possibly generate low-frequency seismicity (e.g. Rust et al., 2008). Shallow hydrothermal systems have
276 been linked to the generation of long-lasting families of earthquakes at ice- or snow-covered volcanoes (e.g.
277 Matoza et al., 2015; Park et al., 2019). Here, the interplay of hydrothermal fluids with seasonal meltwater
278 from above may lead to repeated over-pressurization and failure of a constricted volume within the fluid
279 pathways of an extensive crack system. Indeed, persistent fumarolic activity has often been observed
280 close to, or within the summit vent of Llaima. However, two observations indicate this mechanism may
281 not be occurring: 1) a volumetric source would give the same first motions for waveform arrivals at all
282 stations, but first motions observed here are mixed (Fig. 5), and 2) a volumetric source would be expected
283 to generate low-frequency resonance and thus common spectral peaks would be seen at all stations (e.g.
284 Waite et al., 2008) and this characteristic is not observed here (Fig. 4c). It would be appropriate to carry
285 out a full moment tensor inversion to quantify the source mechanism but the lack of an accurate shallow
286 velocity model prevents us from doing so; further work is needed to calculate a reliable velocity model for
287 shallow depths at Llaima volcano. Nevertheless, until a full moment tensor inversion can be calculated for
288 the families observed here, we cannot exclude hydrothermal fluid activity at Llaima volcano as a possible
289 source for minor repetitive seismic activity around the edifice.

290 Alternatively, slow-slip failure through poorly consolidated volcanic material at shallow depths can also
291 generate seismic activity with high- to low-frequency attenuation patterns (Bean et al., 2013; Heap et al.,
292 2015). Temporally complex deformation was noted on the eastern flank of Llaima volcano prior to or
293 during the 2007-09 eruption, and was inferred to be a result of a potential slow-slip landslide (Fournier
294 et al., 2010). The location of this landslide (approximately 5 km east of station GEO) does not correlate
295 with the locations calculated for the largest families here (Fig. 6) and there have been no studies detailing
296 if deformation in this area had continued up to 2015. Furthermore, data from compaction experiments
297 suggests that failure in poorly consolidated materials such as ash tuffs is unlikely to generate repetitive
298 low-frequency seismicity (Heap et al., 2015). However, with the evidence presented here we cannot

299 completely rule out shallow slow-slip as a potential source of minor seismic activity on other regions of the
300 volcano.

301 For glacial sources of seismicity, there are multiple different mechanisms that have been documented
302 (Podolskiy and Walter, 2016). We can disregard mechanisms involving hydraulic resonance in or below the
303 ice (e.g. Lawrence and Qamar, 1979; Métaixian et al., 2003) because there are no consistent spectral peaks
304 between stations or evidence of harmonics (Fig. 4c), though the resonant character of the signal could
305 be lost due signal alteration in the heterogeneous medium at shallow depths. Furthermore, we observe
306 mixed polarity first motions (Fig. 5) when hydraulic motion might be expected to generate isotropic first
307 motion. [However, in rare cases this type of source could generate mixed polarity first motions if the
308 fluid driven crack involves some complex combination of source mechanisms including shear failure or
309 compensated linear vector dipole (e.g. Waite et al., 2008).] We also exclude mechanisms involving ice-fall
310 or serac collapses (e.g. Jónsdóttir et al., 2009) as the impact of ice onto ground should not be expected to
311 generate mixed polarity first motions. Besides, there are no well documented areas on the glacial ice at
312 Llaima volcano that could host persistent, highly-repetitive ice-fall that could generate the seismic families
313 documented here. Glacial crevassing is the most common type of alpine glacier seismic source (e.g. Neave
314 and Savage, 1970; Walter et al., 2008), and has been documented to generate families of repeating events
315 (e.g. Mikesell et al., 2012). However, this mechanism generates relatively little seismic energy and steep
316 alpine glaciers tend to be poorly coupled to the bedrock (Kamb, 1970), so seismic waves are inefficiently
317 transferred from ice to rock (Weaver and Malone, 1979). As a result, crevassing seismicity are usually only
318 detected by seismic instruments deployed directly onto the ice or on rock in close proximity to the glacier
319 (Weaver and Malone, 1979; Thelen et al., 2013). Again, the mixed polarity first motions present a strong
320 argument against crevassing as it is a volumetric source and should generate isotropic first motions. It is
321 worth noting that our analytical workflow made a key assumption that most of the icequakes that could
322 be occurring at Llaima are of a repetitive and persistent nature. It is possible that there were also many
323 small, non-repetitive seismic events of a glacial origin that were not automatically detected here. Outside
324 of manually and inefficiently picking these possible events from the seismic record, it is not yet feasible to
325 build a catalog of these events.

326 Of all the candidate source mechanisms, basal stick-slip sliding close to or at the interface between ice
327 and rock is the most likely. Repetitive, low-frequency seismicity generated by discrete glacial movements
328 along the base has been well documented (e.g. Weaver and Malone, 1976, 1979; Ekstrom et al., 2003;
329 Caplan-Auerbach and Huggel, 2007; Zoet et al., 2012; Thelen et al., 2013; Allstadt and Malone, 2014). The
330 repetitive, persistent families observed at Llaima volcano (Fig. 2c) require non-destructive and repeatable
331 sources, which can be provided by stick-slip motion over a stationary asperity at the ice-rock interface.
332 Alternatively, stick-slip motion can also be generated by rocks embedded in the ice (i.e. ‘dirty patch’; e.g.
333 Allstadt and Malone, 2014) but the low or stationary motion of the source calculated from CWI (Fig. 7)
334 suggests the former is more likely. The mixed polarity first motions for Family 1 (Fig. 5) are also consistent
335 with shear failure at the source, in agreement with what is inferred to occur during stick-slip motion.
336 Stick-slip behavior requires two conditions be met: 1) friction must decrease with slip velocity, so that the
337 associated acceleration can be sustained, and 2) healing (i.e. strengthening) must occur at the slip interface,
338 so that static stress can be recharged (Zoet and Iverson, 2018). With the latter condition, one effect is
339 that longer time periods without slip would lead to bigger stress build-up and bigger subsequent seismic
340 events, a behavior that is hinted at for Family 1 (Fig. 3b). However, other laboratory experiments have
341 shown that temperature changes can have a significant effect on the strength and stability of ice-on-rock
342 friction (McCarthy et al., 2017). This may explain why we find a weak correlation between the repose
343 interval and the pseudo-energies of the events in Family 1 (Fig. 3b) and very little correlation in the other

344 families (Fig. S3). Laboratory experiments have shown that stick-slip behavior can occur in soft-bedded
345 glaciers (Zoet and Iverson, 2018), which may be a condition beneath the glaciers at Llaima and other
346 ice-covered volcanoes due to eruptive products such as tephra. Lastly, it is important to note that any linear
347 relationships between repose time and seismic event energies (e.g. Fig. 3b) could be explained by other
348 physical mechanisms. For example, it could also be indicative of repeated pressurization and failure of
349 a fluid-driven crack (e.g. Matoza and Chouet, 2010; Matoza et al., 2015). Therefore, while the tangible
350 relationship presented in Fig. 3b is noteworthy, we emphasize that a robust waveform inversion is required
351 before conclusions can be drawn about source mechanisms of the seismicity presented here.

352 Llaima volcano has had at least two permanent seismic stations for monitoring activity since 2006,
353 with more stations added during and after the 2007-09 eruptive episode (Franco et al., 2019). Why have
354 the sequences of low-frequency, low-amplitude families described here not been detailed in previous
355 work or in the OVDAS seismic catalog for the volcano? While icequakes have long been noticed in the
356 seismic record at Llaima volcano, limited resources and time have meant that priority has been given to
357 cataloging only volcanic or nearby tectonic events. Nevertheless, it is likely that the low-energy nature
358 of these seismic events would mean they had relatively low SNR at the permanent stations, thus would
359 be too small to be noticed during manual inspection of the seismic data. This is reflected in the fact that
360 only 2 of the ‘long-period’ events cataloged by OVDAS during this time period matched with detected
361 repeating seismic events (Fig. S2). There is currently no program for automatically searching for repeating
362 seismic events at Llaima, although there are tools currently available or in development for such a use
363 (e.g. REDPy; Hotovec-Ellis and Jeffries, 2016). Longer-term studies have found high variability in the
364 number of icequakes at volcanoes, that often relate to observable changes in glacial behavior or seasonal
365 changes in snow loading or temperature (e.g. Weaver and Malone, 1979; Allstadt and Malone, 2014).
366 These studies also noted that the base of a glacier is a dynamic environment with some time periods more
367 favorable for basal stick-slip behavior than other time periods. Thus, there is a good chance that the seismic
368 station network deployed in early 2015 were coincidentally in the right place at the right time to detect the
369 icequakes at Llaima volcano. As this study only looks at a relatively short two month period at the volcano,
370 it is clear there is a need to expand the analysis to a multi-year scale so that seasonal changes in glacial
371 seismic activity can be constrained. Furthermore, the locations calculated here would be of an unacceptably
372 low quality for the needs of continuous monitoring and risk assessment. Therefore, future deployments
373 at Llaima will need to explore new deployment configurations around the glaciers to help constrain the
374 source locations for such low energy events.

375 The findings detailed in this study have important implications for continuous monitoring at Llaima
376 volcano and other ice-covered volcanoes in Chile. At the time of writing, there are at least 8 permanent
377 broadband seismic stations deployed around Llaima volcano which are collectively producing a significant
378 geophysical dataset. This is one such example of an ever-growing volume of geophysical data that require
379 the design and implementation of efficient tools capable of detecting all signals of interest, particularly
380 immediately prior to eruptive activity. Several studies have designed and tested pattern recognition and
381 machine learning tools for discriminating seismic signals at Llaima volcano, with varying degrees of
382 success (Curilem et al., 2014, 2018). However, these algorithms have been ‘trained’ using seismic catalogs
383 that did not account for the significant overlap in characteristics between low-frequency volcanic signals
384 and glacial events. The observations presented in this study raise the possibility that a significant number
385 of events that were classified as volcanic were actually glacial in origin. Therefore, before new automatic
386 algorithms are developed for seismic data at ice-covered volcanoes, more work is needed to efficiently
387 separate the seismic events of glacial and volcanic origin.

6 CONCLUSIONS

388 Glacially derived seismic events, or icequakes, can share many characteristics used to define low-frequency
389 volcanic earthquakes. Thus, there is a present need to improve our ability for distinguishing between these
390 types of seismic events at active ice-covered volcanoes. Here we present a detailed analysis of two months
391 of broadband seismic data collected at Llaima volcano in early 2015, one of the largest and most active
392 ice-covered volcanoes in Chile. The aim of this analysis was to establish the quantity, characteristics, and
393 locations of any glacially derived seismic events that may have occurred. We detail the presence of at least
394 11 families of repeating seismic events of a low-frequency, low-amplitude nature, the largest of which
395 contained 397 events. Through stacking of waveforms in each family, we are able to calculate approximate
396 locations for 3 of the largest families and results suggest they are located at shallow depths beneath glacial
397 areas around the summit vent. Characteristics of the largest family, particularly the repose interval versus
398 pseudo-energy relation and the mixed polarity first motion arrivals, lead us to conclude that these events
399 were derived from stick-slip motion along the base of a glacier near the summit of the volcano. This study
400 represents the first documented attempt at beginning to quantify the prevalence of icequakes at ice-covered
401 volcanoes in Southern Chile. The observations presented here have clear implications for future studies of
402 volcano-seismicity at Llaima volcano and other ice-covered active volcanoes in Southern Chile. However,
403 these observations are derived from a relatively short time interval (2 months) compared to previous studies
404 of icequakes at other volcanoes which used over a decade of seismic data (Jónsdóttir et al., 2009; Allstadt
405 and Malone, 2014). It is clear there is a need to build on this study by expanding the analysis across the
406 whole seismic archive from not only Llaima volcano, but other ice-covered volcanoes in Southern Chile.

AUTHOR CONTRIBUTIONS

407 ODL carried out the calculation and analysis, and drafted the manuscript. JML helped with the location
408 calculation. LFM and JL provided OVDAS catalog data and weather data. AR provided the data to quantify
409 the location and amount of glacial ice on Llaima. SJL and MJS participated in the design of the study. All
410 authors read and approved the final manuscript.

ACKNOWLEDGMENTS

411 This research was performed while ODL held an NRC Research Associateship with the U.S. Army
412 Research Laboratory/Army Research Office while based at the University of North Carolina at Chapel
413 Hill. The authors wish to thank Dylan T. Mikesell and Rebecca Rodd for help with field data collection
414 and deployment organization in 2015, as well as to Jeffrey B. Johnson, Timothy J. Ronan, and Thomas L.
415 Otheim for their help in the fieldwork. JML acknowledges the support from NSF grants CDI 1125185 and
416 AGS-1551999. The authors would also like to thank Robin Matoza and an anonymous reviewer for their
417 comments and suggestions which helped greatly improve the manuscript.

DATA AVAILABILITY STATEMENT

418 All data presented here will be made available on request to the corresponding author.

REFERENCES

- 419 Allstadt, K. E. and Malone, S. D. (2014). Swarms of repeating stick-slip icequakes triggered by snow
420 loading at Mount Rainier volcano. *Journal of Geophysical Research: Earth Surface* 119, 1180–1203.
421 doi:10.1002/2014JF003086
- 422 Aster, R. C. and Winberry, J. P. (2017). Glacial seismology. *Reports on Progress in Physics* 80. doi:10.
423 1088/1361-6633/aa8473
- 424 Bean, C. J., De Barros, L., Lokmer, I., Métaixian, J.-P., O' Brien, G., and Murphy, S. (2013). Long-period
425 seismicity in the shallow volcanic edifice formed from slow-rupture earthquakes. *Nature Geoscience* 7,
426 71–75. doi:10.1038/ngeo2027
- 427 Bishop, J., Lees, J., Biryol, C. B., Mikesell, T. D., and Franco, L. (2018). Examining the interior of
428 Llaima Volcano with receiver functions. *Journal of Volcanology and Geothermal Research* 352, 1–9.
429 doi:10.1016/j.jvolgeores.2017.11.022
- 430 Buurman, H. and West, M. E. (2013). Magma fracture and hybrid earthquakes in the conduit of Augustine
431 Volcano. *Geophysical Research Letters* 40, 6038–6042. doi:10.1002/2013GL057864
- 432 Caplan-Auerbach, J. and Huggel, C. (2007). Precursory seismicity associated with frequent, large ice
433 avalanches on Iliamna volcano, Alaska, USA. *Journal of Glaciology* 53, 128–140. doi:10.3189/
434 172756507781833866
- 435 Carmichael, J. D. (2013). *Melt-triggered seismic response in hydraulically-active polar ice: Observations
436 and methods*. Phd thesis, University of Washington
- 437 Chouet, B. A. (1996). Long-period volcano seismicity: its source and use in eruption forecasting. *Nature*
438 380, 309–316. doi:10.1038/380309a0
- 439 Chouet, B. A. and Matoza, R. S. (2013). A multi-decadal view of seismic methods for detecting precursors
440 of magma movement and eruption. *Journal of Volcanology and Geothermal Research* 252, 108–175.
441 doi:10.1016/j.jvolgeores.2012.11.013
- 442 Curilem, M., Huenupan, F., Beltrán, D., San Martín, C., Fuentealba, G., Franco, L., et al. (2014). Pattern
443 recognition applied to seismic signals of Llaima volcano (Chile): An evaluation of station-dependent
444 classifiers. *Journal of Volcanology and Geothermal Research* 282, 134–147. doi:10.1016/j.jvolgeores.
445 2016.02.006
- 446 Curilem, M., Mello, R., Huenupan, F., San Martín, C., Franco, L., Hernández, E., et al. (2018).
447 Discriminating seismic events of the Llaima volcano (Chile) based on spectrogram cross-correlations.
448 *Journal of Volcanology and Geothermal Research* 367, 63–78. doi:10.1016/J.JVOLGEORES.2018.10.
449 023
- 450 Danesi, S., Bannister, S., and Morelli, A. (2007). Repeating earthquakes from rupture of an asperity under
451 an Antarctic outlet glacier. *Earth and Planetary Science Letters* 253, 151–158. doi:10.1016/j.epsl.2006.
452 10.023
- 453 de Maisonrouve, C. B., Dungan, M. A., Bachmann, O., and Burgisser, A. (2012). Insights into shallow
454 magma storage and crystallization at Volcán Llaima (Andean Southern Volcanic Zone, Chile). *Journal
455 of Volcanology and Geothermal Research* 211–212, 76–91. doi:10.1016/j.jvolgeores.2011.09.010
- 456 Douma, H. and Snieder, R. (2006). Correcting for bias due to noise in coda wave interferometry.
457 *Geophysical Journal International* 164, 99–108. doi:10.1111/j.1365-246X.2005.02807.x
- 458 Ekstrom, G., Nettles, M., and Abers, G. A. (2003). Glacial Earthquakes. *Science* 302, 622–624.
459 doi:10.1126/science.1088057
- 460 Fournier, T. J., Pritchard, M. E., and Riddick, S. N. (2010). Duration, magnitude, and frequency of
461 subaerial volcano deformation events: New results from Latin America using InSAR and a global
462 synthesis. *Geochemistry, Geophysics, Geosystems* 11. doi:10.1029/2009GC002558

- 463 Franco, L., Palma, J. L., Lara, L. E., Gil-Cruz, F., Cardona, C., Basualto, D., et al. (2019). Eruptive
464 sequence and seismic activity of Llaima volcano (Chile) during the 2007–2009 eruptive period: Inferences
465 of the magmatic feeding system. *Journal of Volcanology and Geothermal Research* 379, 90–105.
466 doi:10.1016/j.jvolgeores.2019.04.014
- 467 Heap, M. J., Kennedy, B. M., Pernin, N., Jacquemard, L., Baud, P., Farquharson, J. I., et al. (2015).
468 Mechanical behaviour and failure modes in the Whakaari (White Island volcano) hydrothermal system,
469 New Zealand. *Journal of Volcanology and Geothermal Research* 295, 26–42. doi:10.1016/j.jvolgeores.
470 2015.02.012
- 471 Helmstetter, A., Moreau, L., Nicolas, B., Comon, P., and Gay, M. (2015). Intermediate-depth icequakes and
472 harmonic tremor in an Alpine glacier (Glacier d'Argentière, France): Evidence for hydraulic fracturing?
473 *Journal of Geophysical Research: Earth Surface* 120, 402–416. doi:10.1002/2014JF003289
- 474 Hotovec-Ellis, A. J. and Jeffries, C. (2016). Near Real-time Detection, Clustering, and Analysis of
475 Repeating Earthquakes: Application to Mount St. Helens and Redoubt Volcanoes. In *Seismological*
476 *Society of America Annual Meeting*
- 477 Iverson, R. M., Dzurisin, D., Gardner, C. A., Gerlach, T. M., LaHusen, R. G., Lisowski, M., et al. (2006).
478 Dynamics of seismogenic volcanic extrusion at Mount St Helens in 2004–05. *Nature* 444, 439–43.
479 doi:10.1038/nature05322
- 480 Jónsdóttir, K., Roberts, R., Pohjola, V., Lund, B., Shomali, Z. H., Tryggvason, A., et al. (2009). Glacial
481 long period seismic events at Katla volcano, Iceland. *Geophysical Research Letters* 36, L11402.
482 doi:10.1029/2009GL038234
- 483 Kamb, B. (1970). Sliding motion of glaciers: Theory and observation. *Reviews of Geophysics* 8, 673.
484 doi:10.1029/RG008i004p00673
- 485 Kendrick, J. E., Lavallée, Y., Hirose, T., Di Toro, G., Hornby, A. J., De Angelis, S., et al. (2014). Volcanic
486 drumbeat seismicity caused by stick-slip motion and magmatic frictional melting. *Nature Geoscience* 7,
487 438–442. doi:10.1038/NGEO2146
- 488 Lahr, J. C., Chouet, B. A., Stephens, C. D., Power, J. A., and Page, R. A. (1994). Earthquake classification,
489 location, and error analysis in a volcanic environment: implications for the magmatic system of the
490 1989–1990 eruptions at Redoubt Volcano, Alaska. *Journal of Volcanology and Geothermal Research* 62,
491 137–151
- 492 Lamb, O. D., De Angelis, S., Umakoshi, K., Hornby, A. J., Kendrick, J. E., and Lavallée, Y. (2015).
493 Repetitive fracturing during spine extrusion at Unzen volcano, Japan. *Solid Earth* 6, 1277–1293.
494 doi:10.5194/se-6-1277-2015
- 495 Lawrence, W. S. and Qamar, A. (1979). Hydraulic Transients: A Seismic Source in Volcanoes and Glaciers.
496 *Science* 203, 654–656. doi:10.1126/science.203.4381.654
- 497 Lesage, P., Heap, M. J., and Kushnir, A. (2018). A generic model for the shallow velocity structure of
498 volcanoes. *Journal of Volcanology and Geothermal Research* 356, 114–126. doi:10.1016/j.jvolgeores.
499 2018.03.003
- 500 Matoza, R. S. and Chouet, B. A. (2010). Subevents of long-period seismicity: Implications for hydrothermal
501 dynamics during the 2004–2008 eruption of Mount St. Helens. *Journal of Geophysical Research* 115,
502 B12206. doi:10.1029/2010JB007839
- 503 Matoza, R. S., Chouet, B. A., Dawson, P. B., Shearer, P. M., Haney, M. M., Waite, G. P., et al. (2015).
504 Source mechanism of small long-period events at Mount St. Helens in July 2005 using template matching,
505 phase-weighted stacking, and full-waveform inversion. *Journal of Geophysical Research: Solid Earth*
506 120, 6351–6364. doi:10.1002/2015JB012279

- 507 McCarthy, C., Savage, H., and Nettles, M. (2017). Temperature dependence of ice-on-rock friction at
508 realistic glacier conditions. *Philosophical Transactions of the Royal Society A: Mathematical, Physical*
509 *and Engineering Sciences* 375, 20150348. doi:10.1098/rsta.2015.0348
- 510 Métaixian, J.-P., Araujo, S., Mora, M. M., and Lesage, P. (2003). Seismicity related to the glacier of
511 Cotopaxi Volcano, Ecuador. *Geophysical Research Letters* 30, 1–4. doi:10.1029/2002GL016773
- 512 Mikesell, T. D., Wijk, K. V., Haney, M. M., Bradford, J. H., Marshall, H. P., and Harper, J. T. (2012).
513 Monitoring glacier surface seismicity in time and space using Rayleigh waves. *Journal of Geophysical*
514 *Research* 117, 1–12. doi:10.1029/2011JF002259
- 515 Mora-Stock, C., Thorwart, M., Wunderlich, T., Bredemeyer, S., Hansteen, T. H., and Rabbel, W. (2014).
516 Comparison of seismic activity for Llaima and Villarrica volcanoes prior to and after the Maule 2010
517 earthquake. *International Journal of Earth Sciences* 103, 2015–2028. doi:10.1007/s00531-012-0840-x
- 518 Naranjo, J. A. and Moreno, H. (2005). Geología del Volcán Llaima. *Carta Geológica de Chile - Serie*
519 *Geología Básica* 88, 1–37
- 520 Neave, K. G. and Savage, J. C. (1970). Icequakes on the Athabasca Glacier. *Journal of Geophysical*
521 *Research* 75, 1351–1362. doi:10.1029/JB075i008p01351
- 522 Neuberg, J. W., Tuffen, H., Collier, L., Green, D. N., Powell, T., and Dingwell, D. B. (2006). The trigger
523 mechanism of low-frequency earthquakes on Montserrat. *Journal of Volcanology and Geothermal*
524 *Research* 153, 37–50. doi:10.1016/j.jvolgeores.2005.08.008
- 525 Park, I., Jolly, A., Kim, K. Y., and Kennedy, B. (2019). Temporal variations of repeating low frequency
526 volcanic earthquakes at Ngauruhoe Volcano, New Zealand. *Journal of Volcanology and Geothermal*
527 *Research* 373, 108–119. doi:10.1016/j.jvolgeores.2019.01.024
- 528 Paul, F., Barrand, N., Baumann, S., Berthier, E., Bolch, T., Casey, K., et al. (2013). On the accuracy of
529 glacier outlines derived from remote-sensing data. *Annals of Glaciology* 54, 171–182. doi:10.3189/
530 2013AoG63A296
- 531 Podolskiy, E. A. and Walter, F. (2016). Cryoseismology. *Reviews of Geophysics* S4, 708–758. doi:10.
532 1002/2016RG000526
- 533 Reinthaler, J., Paul, F., Granados, H. D., Rivera, A., and Huggel, C. (2019). Area changes of glaciers
534 on active volcanoes in Latin America between 1986 and 2015 observed from multi-temporal satellite
535 imagery. *Journal of Glaciology* , 1–15, doi:10.1017/jog.2019.30
- 536 Roeoesli, C., Helmstetter, A., Walter, F., and Kissling, E. (2016). Meltwater influences on deep stick-slip
537 icequakes near the base of the Greenland Ice Sheet. *Journal of Geophysical Research: Earth Surface*
538 121, 223–240. doi:10.1002/2015JF003601
- 539 Rowe, C. A., Aster, R. C., Borchers, B., and Young, C. J. (2002). An Automatic, Adaptive Algorithm for
540 Refining Phase Picks in Large Seismic Data Sets. *Bulletin of the Seismological Society of America* 92,
541 1660–1674. doi:10.1785/0120010224
- 542 Rust, A. C., Balmforth, N. J., and Mandre, S. (2008). The feasibility of generating low-frequency volcano
543 seismicity by flow through a deformable channel. *Geological Society, London, Special Publications* 307,
544 45–56. doi:10.1144/SP307.4
- 545 Senobari, N. S., Funning, G. J., Keogh, E., Zhu, Y., Yeh, C. M., Zimmerman, Z., et al. (2019). Super-
546 Efficient Cross-Correlation (SEC-C): A Fast Matched Filtering Code Suitable for Desktop Computers.
547 *Seismological Research Letters* 90, 322–334. doi:10.1785/0220180122
- 548 Snieder, R., Gret, A., Douma, H., and Scales, J. (2002). Coda Wave Interferometry Estimating Nonlinear
549 Behaviour in Seismic Velocity. *Science* 295, 2253–2255. doi:10.1126/science.1070015

- 550 Snieder, R. and Vrijlandt, M. (2005). Constraining the source separation with coda wave interferometry:
551 Theory and application to earthquake doublets in the Hayward fault, California. *Journal of Geophysical*
552 *Research* 110, 2156–2202. doi:10.1029/2004JB003317
- 553 Soto, R., Huenupan, F., Meza, P., Curilem, M., and Franco, L. (2018). Spectro-temporal features applied
554 to the automatic classification of volcanic seismic events. *Journal of Volcanology and Geothermal*
555 *Research* 358, 194–206. doi:10.1016/j.jvolgeores.2018.04.025
- 556 Thelen, W. A., Allstadt, K. E., De Angelis, S., Malone, S. D., Moran, S. C., and Vidale, J. (2013). Shallow
557 repeating seismic events under an alpine glacier at Mount Rainier, Washington, USA. *Journal of*
558 *Glaciology* 59, 345–356. doi:10.3189/2013JoG12J111
- 559 Venzke, E. (2013). *Global Volcanism Program*. doi:10.5479/si.GVP.VOTW4-2013
- 560 Völker, D., Kutterolf, S., and Wehrmann, H. (2011). Comparative mass balance of volcanic edifices at the
561 southern volcanic zone of the Andes between 33°S and 46°S. *Journal of Volcanology and Geothermal*
562 *Research* 205, 114–129. doi:10.1016/j.jvolgeores.2011.03.011
- 563 Waite, G. P., Chouet, B. A., and Dawson, P. B. (2008). Eruption dynamics at Mount St. Helens imaged
564 from broadband seismic waveforms: Interaction of the shallow magmatic and hydrothermal systems.
565 *Journal of Geophysical Research* 113, 1–22. doi:10.1029/2007JB005259
- 566 Walter, F., Deichmann, N., and Funk, M. (2008). Basal icequakes during changing subglacial water
567 pressures beneath Gornergletscher, Switzerland. *Journal of Glaciology* 54, 511–521. doi:10.3189/
568 002214308785837110
- 569 Weaver, C. S. and Malone, S. D. (1976). Mt. Saint Helens Seismic Events: Volcanic Earthquakes or Glacial
570 Noises? *Geophysical Research Letters* 3, 197–200
- 571 Weaver, C. S. and Malone, S. D. (1979). Seismic Evidence for Discrete Glacier Motion at the Rock–Ice
572 Interface. *Journal of Glaciology* 23, 171–184. doi:10.1017/S0022143000029816
- 573 West, M. E., Larsen, C. F., Truffer, M., O’Neel, S., and LeBlanc, L. (2010). Glacier microseismicity.
574 *Geology* 38, 319–322. doi:10.1130/G30606.1
- 575 Zoet, L. K., Anandakrishnan, S., Alley, R. B., Nyblade, A. A., and Wiens, D. A. (2012). Motion
576 of an Antarctic glacier by repeated tidally modulated earthquakes. *Nature Geoscience* 5, 623–626.
577 doi:10.1038/ngeo1555
- 578 Zoet, L. K. and Iverson, N. R. (2018). A healing mechanism for stick-slip of glaciers. *Geology* 46, 807–810.
579 doi:10.1130/G45099.1